

Original article

An experimental study of imbibition process and fluid distribution in tight oil reservoir under different pressures and temperatures

Yisheng Liang^{1,2}, Fengpeng Lai^{1,2}*, Yuting Dai^{1,2}, Hao Shi^{1,2}, Gongshuai Shi^{1,2}

¹School of Energy Resources, China University of Geosciences (Beijing), Beijing 100083, P. R. China

²Beijing Key Laboratory of Unconventional Natural Gas Geological Evaluation and Development Engineering, Beijing 100083, P. R. China

Keywords:

Imbibition
tight reservoir
fluid distribution
pore-size distribution

Cited as:

Liang, Y., Lai, F., Dai, Y., Shi, H., Shi, G.
An experimental study of imbibition process and fluid distribution in tight oil reservoir under different pressures and temperatures. *Capillarity*, 2021, 4(4): 66-75, doi: 10.46690/capi.2021.04.02

Abstract:

Tight reservoirs are a major focus of unconventional reservoir development. As a means to improve hydrocarbon recovery from tight reservoirs, imbibition has been received increasing attentions in recent years. This study evaluates how the changes in temperature and pressure affect imbibition through conducting experimental tests under various conditions on samples from the Yan Chang formation, a tight reservoir in Ordos Basin. The fluid distribution is compared before and after imbibition in core samples by nuclear magnetic resonance method. The results show that the imbibition recovery is significantly improved through increasing temperature and pressure. A high temperature facilitates molecular thermal movements, increasing oil-water exchange rate. The core samples are characterized with nano-mesopores, which is followed by nano-macropores, micropores, mesopores, and nano-micropores. Comparative analysis of nuclear magnetic resonance shows that the irreducible water saturation increases after imbibition and is mainly distributed in nanopores. Increasing pressure increases the amount of residual water in nano pores, with the relatively more significant increase in the amount of residual water in nanomacropores compared with other types of pores.

1. Introduction

Tight-oil resources contribute a significant portion to the unconventional resources in China. It is reported that by 2018, China's unconventional oil resources were 672.08×10^8 t, among which tight oil resources accounted for 125.80×10^8 t (Zou et al., 2018). Because of the tiny pore throat and high capillary force, evaluating the imbibition behaviors is of great significance to improve oil recovery from tight reservoirs.

Previous imbibition studies can be categorized into theoretical and experimental research to evaluate mechanisms of imbibition in tight reservoirs. The theoretical models of spontaneous imbibition are generally divided into two groups, one is the piston water-displacement model based on Hagen-Posieuille equation (Washburn, 1921; Wang and Sheng, 2020), and the other is non-piston waterflooding model, based on

the partial discharge equation (McWhorter and Sunada, 1990; Schmid et al., 2013). The theoretical model of spontaneous imbibition can be expressed with dimensionless time, and the experimental data are typically normalized to upscale to reservoir conditions. Aronofsky and Jenkins (1954) established an empirical model of spontaneous imbibition to describe the variation of spontaneous imbibition efficiency with imbibition time. Many scholars have thereby modified the empirical model. Among them, Ma et al. (1997) and Mason et al. (2010) considered the influence of wetting-phase fluid viscosity on imbibition. Several studies have further examined the effects of boundary conditions, gravity, initial water saturation, and surfactant on spontaneous imbibition (Zhang et al., 1996; Babadagli, 2002; Li et al., 2002; Mason et al., 2010; Nasralla et al., 2013). Cai et al. (2014) modified the spontaneous-imbibition model by considering pore size, pore shape, and

tortuosity of the imbibition streamline. Gao and Hu (2015) studied the effects of median pore-throat diameter on spontaneous imbibition, and proposed a new scaling equation to compensate for the relationship between median pore-throat diameter and imbibition. A general scaling equation was used to describe the countercurrent spontaneous imbibition process (Schmid et al., 2011). Ghasemi et al. (2020) studied the influence of various factors on gas reservoir imbibition, and introduced a new scale equation, which can be used to accurately predict the imbibition in gas reservoir. Shen et al. (2020) established an analytical model which describes the capillary rise in nano-channels by considering inherent surface roughness, and reported a good agreement between the model and experimental results. Their model provided an option to predict imbibition through using their relationship between imbibition height and time. Xu et al. (2021) found that the traditional models can significantly deviate from experimental data, and proposed to couple the factors of fluid and reservoir into imbibition model. Gong et al. (2021) proposed a new full dynamic pore network modeling platform, which can be used to study the pore scale under various two-phase flow conditions in fractures, and their findings have extended implications for predictions of capillary trapping behavior in fractured media.

They studied the effect of different surfactants on interfacial tension, so as to improve oil recovery rate and recovery (Schechter et al., 1994; Adibhatla and Mohanty, 2008; Mohammadi et al., 2019). Yildiz et al. (2006) analyzed the influence of shape factor and boundary conditions on spontaneous imbibition. Akbarabadi and Piri (2014) conducted sorption experiments with brine, surfactant and oil. Yang et al. (2015) studied the relationship between imbibition characteristics, pore connectivity and pore-size distribution. Lai et al. (2016) studied the effects of boundary conditions, wettability, temperature, and oil viscosity on water absorption. Cai et al. (2020) studied the effects of salinity and mineral composition on self absorption by conducting a series of imbibition experiments on four kinds of dense sandstones with different mineral contents, and systematically changing salinity to study its effects on Imbibition capacity and permeability. Dynamic imbibition is a type of spontaneous imbibition when the external liquid is flowing, that is, the water has a certain injection speed. To study the influence of different boundaries on imbibition, Meng and Cai (2018) reviewed the imbibition research at core scale, analyzed the relative permeability of imbibition, and finally discussed the analysis model of imbibition. Previous

results show that the dynamic imbibition efficiency firstly increases and then decreases with increasing displacement velocity, and reaches a dynamic balance between imbibition and displacement at a flow rate of 0.04 mL/min, which is also the flow rate at which the imbibition efficiency is maximized. Dou et al. (2020) studied the dynamic imbibition displacement mechanism of a tight sandstone reservoir in the Yan Chang Formation of the Ordos Basin. They reported an optimal displacement rate in dynamic imbibition displacement, and showed that the optimal displacement rate increases almost linearly with the increase in core permeability. Their results provided theoretical guidance for the optimization and improvement of the water-injection technology in tight sandstone reservoirs. Comparing the pros and cons of imbibition under static and dynamic conditions, studies have evaluated the influences of fluid type, fluid concentration, fluid injection volume, displacement velocity, reaction time, and core permeability on the imbibition displacement efficiency, and these studies have determined the optimum dynamic imbibition displacement velocity (Fini et al., 2012; Dou et al., 2021; Hu et al., 2021).

Previous studies mainly focused on the imbibition at macro-scale. However, it remains uncertain about how temperature and pressure affect imbibition at micro-scale, and the fluid distribution in the pores of tight reservoirs. In this study, imbibition experiments were conducted under various conditions of temperature and pressure on core samples collected from Yan Chang Formation, a tight reservoir in the Ordos Basin. The fluid distribution in the pore network of core samples was further evaluated by nuclear magnetic resonance (NMR) method before and after imbibition.

2. Experiments

2.1 Materials

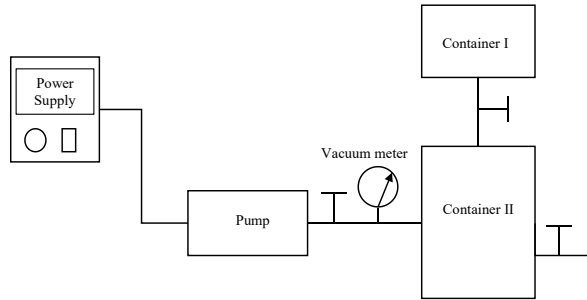
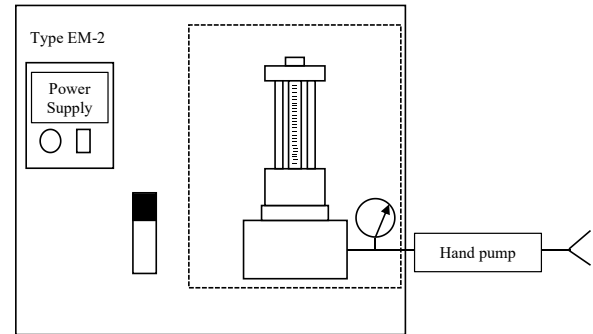
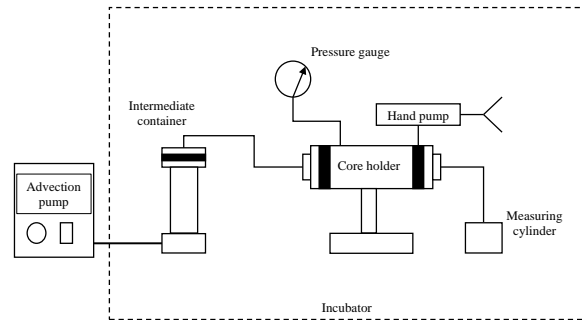
Fig. 1 shows the six core samples collected from the Yan Chang Formation. Before the experiment, the cores were cleaned by ultrasonic for 1 h, and then washed with distilled water. The samples were placed in a drying oven, and the temperature was set under 105 °C for 24 h. After the samples being cooled down to room temperature, the length (L) and the diameter (D) of samples were measured. The cores were then weighed by an electronic balance, and the weight was recorded as M . Table 1 summaries the key information of six samples. In order to simulate the formation condition, 2000 mL of formation water was prepared. Dehydrogenated kerosene was employed to replace oil in the experiment.



Fig. 1. Six core samples used in this study.

Table 1. Basic parameters of six samples.

No.	Diameter (cm)	Length (cm)	Volume (cm ³)	Porosity (%)	Permeability (mD)
S1	2.47	3.04	14.56	4.81	0.08
S2	2.47	3.13	14.98	10.39	0.09
S3	2.50	4.06	19.92	4.06	0.04
S4	2.50	4.00	19.63	4.00	0.06
S5	2.50	3.07	15.06	4.67	0.03
S6	2.50	3.04	14.92	5.72	0.06

**Fig. 2.** Vacuum and pressure saturation device.**Fig. 4.** Schematics of the high temperature and pressure suction device.**Fig. 3.** Schematics of device for the displacement experiments.

2.2 Vacuum and pressure saturation experiment

The saturated water in the sample was replaced by dehydrogenated kerosene to obtain the rock sample with saturated oil and irreducible water. Then, the treated samples and the simulated formation water were placed into a vacuum device (Figs. 2 and 3). The device was vacuumed for 12 h to discharge the air in the device. The pressure valve was opened, formation water was injected and the saturation pressure was set to 20 MPa. With negative pressure in core and 20 MPa of pressure in the device, the simulated formation water entered the core through pore channels. This process lasted for 24 h. After pressure saturation, rock samples were taken and placed in simulated formation water containers for further use.

The displacement experiment was conducted in the following four key steps:

- 1) The flow rate was set at 0.01 mL/min, and the intermediate container was filled with dehydrogenated kerosene.

- 2) The core was placed in the core holder and the confining pressure was set to 8 MPa.
- 3) A small measuring cylinder was connected at the device end to measure the amount of the displaced water.
- 4) After performing the displacement experiment for 24 h, the core was removed from the support and the liquid on the surface was wiped off. After the experiment, the rock sample was placed in a dehydrogenated kerosene bottle for further usage.

2.3 Imbibition experiments under different temperatures and pressures

Fig. 4 shows the schematics of the high temperature and pressure imbibition device. After the sample being saturated in oil, it was placed in the imbibition device and changed the external pressure and temperature. The imbibition curves under the temperature of 20 °C/60 °C and pressure of 0.1 MPa/4 MPa were compared, respectively. Only one variable was changed at a time. Different temperatures and pressures were combined to form different experimental conditions. After the imbibition experiment started, the imbibition state at different time was recorded outside the instrument. The change of instrument indication in the imbibition device reflected the degree of imbibition. Meanwhile, to mimic the imbibition process under formation condition, 2000 mL of the formation water was prepared with a density of 1.2 g/cm³.

The specific experimental steps were as follows

- 1) The rock sample was placed in the imbibition bottle and set the corresponding temperature and pressure.
- 2) The observation interval was increased from 5 min to 10 min, 20 min, and 1 h.

- 3) After 24 hours of core imbibition, the pressure and temperature of the imbibition instrument are released and the core is taken out.
- 4) By dividing the oil volume obtained at the end of the imbibition experiment by the oil volume obtained from the displacement experiment, the imbibition recovery was obtained.
- 5) After imbibition, the core was put into the NMR instrument to obtain the T_2 spectrum. For the rest of the cores, the experimental steps above were repeated.

2.4 NMR experiment

The samples were put into the NMR device to obtain the T_2 spectrum under different states after the above-mentioned experiments, reflecting the fluid distribution in the pores under different states (Tinni et al., 2015; Lai et al., 2019). By comparing the distribution of pore fluid after imbibition under different conditions, the distribution of the pore fluid under different temperature and pressure conditions was obtained.

Because the principle of NMR experiment is to detect the distribution of H^+ ions, the use of dehydrogenated kerosene in the experiment can avoid detection, and the response in the NMR thus mainly reflects the dynamics of water flow. The specific experimental steps were summarized as follows.

- 1) Before the NMR experiment, the sample was gently wiped with a paper towel to remove the fluid on the core surface to prevent the fluid from affecting the experimental results.
- 2) The core to be tested was put into a tube, which was placed into the NMR instrument. The relevant scanning times and frequency offset were set.
- 3) After scanning, the core was taken out from the tube and put into the empty bottle for further usage.
- 4) The T_2 spectrum data obtained after the end of the NMR experiment were processed, exported, and recorded.

3. Experimental results

By comparing the curves of the relationship between the recovery rate and time under different conditions, the influence of temperature and pressure on the imbibition was obtained. Table 2 shows the imbibition recovery under different conditions. Under 20 °C and 0.1 MPa, the recovery ranges from 16.10% to 26.44%, with an average value of 22.90%. With the increase in the temperature or pressure, the recovery is

Table 2. Final recovery of imbibition.

No.	Imbibition recovery		
	20 °C 0.1 MPa (%)	20 °C 4 MPa (%)	60 °C 4 MPa (%)
S1	20.30	21.92	28.1
S2	26.25	26.85	29.30
S3	16.10	18.66	36.38
S4	23.97	24.63	30.21
S5	24.39	25.24	33.21
S6	26.44	27.15	36.10

Table 3. Imbibition experiment results of rock samples under 4 MPa and 60 °C (part).

Time (min)	Volume (mL)		Recovery (%)	
	S1	S3	S1	S3
10	0	0	0	0
20	0.001	0.012	0.30	2.15
60	0.008	0.019	2.42	4.04
720	0.055	0.097	16.67	20.63
2000	0.092	0.151	28.10	32.12
5000	0.093	0.171	28.10	36.38
6000	0.094	0.172	28.10	36.38

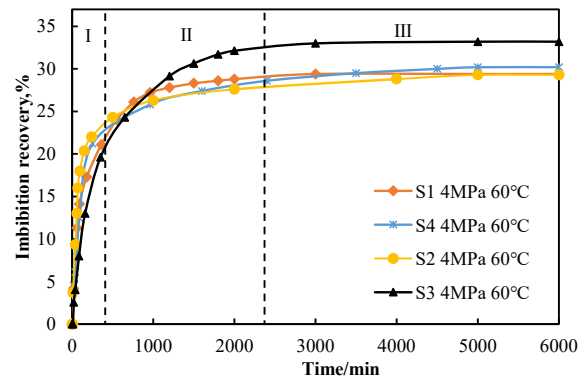


Fig. 5. Imbibition curves of recovery against time for Samples S1, S2, S3, and S4 under 4 MPa and 60 °C.

improved to different degrees, and the increase in the recovery with increasing temperature is the most evident.

3.1 Imbibition curves under 60 °C and 4 MPa

Table 3 shows the imbibed volume and recovery for the samples of S1 and S3 under 60 °C and 4 MPa. Fig. 5 shows the imbibition curves of recovery against time for samples S1, S2, S3, and S4 under 4 MPa and 60 °C. The results show that the imbibition curves can be divided into three stages. The imbibition recovery is most obvious in Stage I. The imbibition curve is relatively smooth and steadily rises in Stage II, and the results show a slower increase in recovery compared with Stage I. In Stage III, the recovery almost remains constant, and the imbibition is almost completed. Meanwhile, the results show an upward trend in the imbibition recovery under the condition of a certain temperature and pressure compared with that under normal temperature and pressure conditions. One may expect that the increase in the temperature reduces the viscosity of the crude oil to a certain extent, which is conducive to the oil-water exchange of fluid in micro pores, that results in the increasing the imbibition recovery.

3.2 Imbibition under 4 MPa and 0.1 MPa

Tables 4 and 5 list the change in the volume of the separated oil in the imbibition instrument at the conditions of 0.1 and 4 MPa, respectively. The results show that the

Table 4. Imbibition experiment results of rock samples under 0.1 MPa and 20 °C (part).

Time (min)	Volume (mL)				Recovery (%)			
	S1	S2	S3	S4	S1	S2	S3	S4
5	0	0	0	0	0	0	0	0
360	0.035	0.03	0.001	0.035	10.61	3.75	0.21	6.6
960	0.04	0.05	0.003	0.045	12.12	6.25	0.64	8.49
4000	0.06	0.16	0.043	0.15	19.20	20.00	10.21	22.0
4500	0.095	0.17	0.063	0.16	19.40	21.25	15.81	22.1
5000	0.095	0.19	0.079	0.18	20.30	23.75	15.96	23.96
6000	0.095	0.21	0.079	0.183	20.30	26.25	16.10	23.97

Table 5. Imbibition experiment results of rock samples under 4 MPa and 20 °C (part).

Time (min)	Volume (mL)				Recovery (%)			
	S1	S2	S3	S4	S1	S2	S3	S4
5	0	0	0	0	0	0	0	0
360	0.001	0.04	0.001	0.001	0.30	3.75	0.21	0.19
960	0.008	0.06	0.003	0.004	2.42	6.25	0.64	0.75
4000	0.055	0.18	0.048	0.051	16.67	20.00	10.21	9.62
4500	0.072	0.19	0.079	0.087	21.89	21.25	16.81	16.42
5000	0.073	0.20	0.083	0.1305	21.92	23.75	17.66	24.62
6000	0.074	0.22	0.083	0.1307	21.92	26.85	17.66	24.63

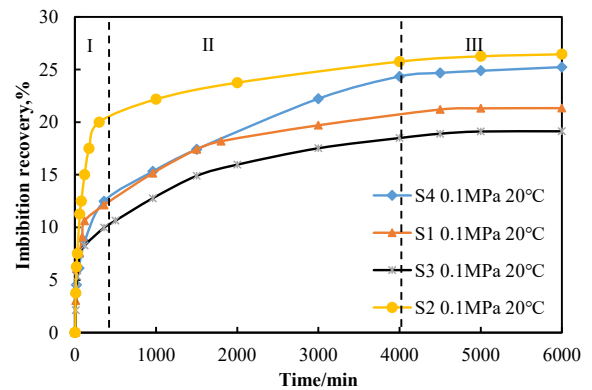
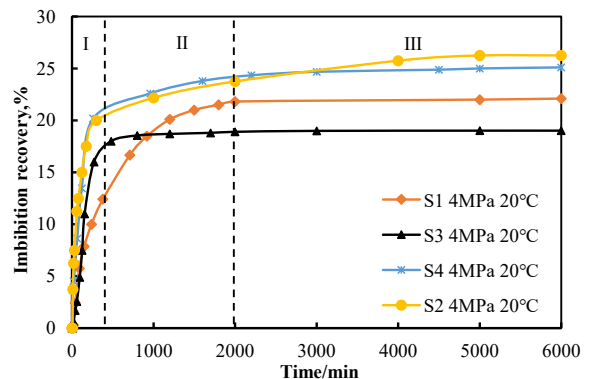
imbibition rate proceeds from fast to slow in the early 360 min, while the oil volume varies greatly with a high imbibition rate after 360 min, where the speed slows down until it is stable.

Figs. 6 and 7 show that the imbibition recovery is around 17-26%. Based on the curve shape, the imbibition process is divided into three regions. The results show insignificant increment in imbibition recovery but significant difference in imbibition rate as pressure changes from 0.1 to 4 MPa. As shown in Figs. 6 and 7, Stage II of samples under 4 MPa ends at around 2000 min, while Stage II of samples under 0.1 MPa ends at around 4000 min. Meanwhile, the imbibition rate of all cores increases, and a higher imbibition rate is achieved. The average imbibition rate is 7.01×10^{-5} mL/min under 0.1 MPa, while the imbibition rate increases to 7.97×10^{-5} mL/min under 4 MPa. One may expect that pressure may affect the capillary pressure between the oil and water phase in the pore throat, and increasing the confining pressure will affect the imbibition by affecting the capillary pressure in the pore throat (Wang et al., 2020).

4. Discussions

4.1 Effects of temperature on imbibition recovery

In this section, the data of the imbibition experiments at 20 °C and 4 MPa and 60 °C and 4 MPa are presented and analyzed to determine the influence of temperature on the imbibition. Fig. 8 presents a comparison of the imbibition recovery of the samples S1 and S2 under the experimental conditions of 4 MPa under 20 °C and 4 MPa under 60 °C.

**Fig. 6.** The imbibition curves of recovery against time for samples S1 to S4 under 0.1 MPa and 20 °C.**Fig. 7.** The imbibition curves of recovery against time for samples S1 to S4 under 4 MPa and 20 °C.

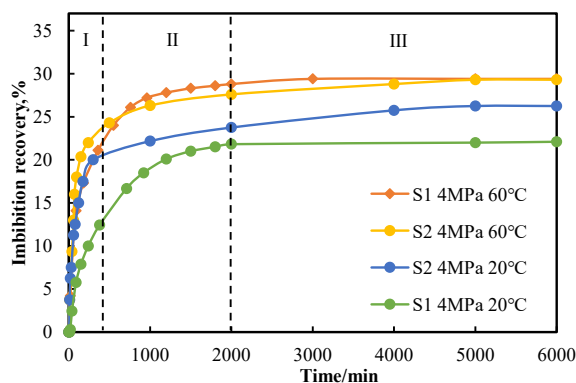


Fig. 8. Comparison of imbibition recovery curves under different temperature conditions.

As shown in Fig. 8, the imbibition recovery improves as temperature increases. The recovery curve of the same core under 60 °C is above that of the 20 °C curve, indicating that the imbibition effect is more significant under 60 °C. In Stage I, the imbibition recovery of core S1 increases by 7% and the imbibition recovery of S2 increases by 5%, which indicates that temperature also plays an important role in the initial stage of imbibition. The curve rises slowly in Stage II, and the imbibition basically ends in Stage III.

As temperature increases from 20 to 60 °C, the recovery of S1 increases from 22.1% to 29.4%, and that of S2 increases from 26.25% to 29%. In other words, an increase in the temperature gradually increases the imbibition recovery, which is consistent with the variation of crude oil viscosity with temperature. From the perspective of thermodynamics and molecular dynamics, when the temperature is increased, the heat absorbed by the crude oil is transformed into kinetic energy between molecules. The thermal motion of molecules is accelerated, and the macro performance or the viscosity of the crude oil decreases, which makes it easier for crude oil to flow between formations, thus promoting the imbibition process. An increase in the temperature results in the thermal expansion of the core's matrix, which leads to the decrease in the size of some pores in the core. The capillary force is the main driving force of imbibition, the pore size of the core becomes smaller, the capillary force is increased, and the formation crude oil expands by heating, which promotes the recovery.

The increase in temperature may somehow change the rock wettability, which can be tested by measuring the contact angles. Studies have reported that increasing temperature increases the wettability angle and the hydrophilicity of the core, contributing to an improved recovery (Sohi et al., 2009; Hendraningrat and Torsæter, 2014). The increase in temperature reduces the interfacial tension, leading to an increased recovery. The increase in temperature may slightly decrease capillary force. However, the decrease in capillary force is expected to be negligible in improving oil recovery compared with other factors (Sohi et al., 2009).

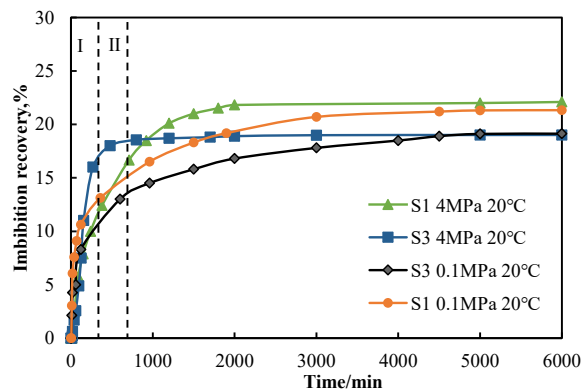


Fig. 9. Comparison of imbibition recovery and time curves of some cores under different pressure conditions.

4.2 Effects of pressure on imbibition recovery

Fig. 9 shows the relationship between imbibition recovery and time under different pressures in some cores. The imbibition recovery of the core under a pressure of 4 MPa is better than that of under 0.1 MPa. The internal structure of the rock is deformed slightly by the increasing of the pressure. The capillary force becomes stronger. Due to compaction, the oil in the nanoscale pores is discharged, resulting in an increase in the core imbibition recovery.

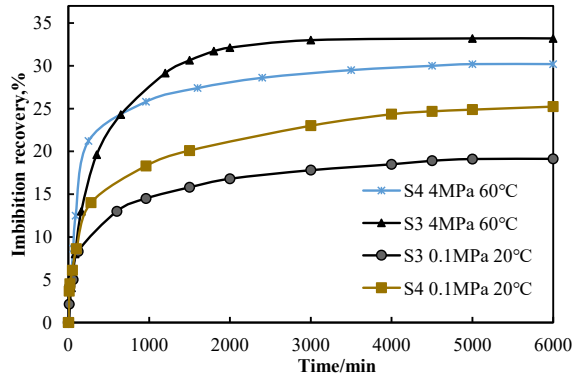
In area I, the recovery curve of the S3 core under 20 °C and 0.1 MPa is higher than 20 °C and 4 MPa curve at 100 min before the start of imbibition, and the increase in the rise of the 20 °C and 4 MPa imbibition curve is greater than that of the 0.1 MPa curve 100 min after the start of imbibition. Similarly, in area II, S1 shows a similar trend to S3 when the imbibition lasts for 500 minutes. The reason for this is that during the rise in the imbibition rate, the formation water enters the small pores in the core. Increasing confining pressure is expected to change the structure of small to medium-size pores in the core, affecting the capillary force which further improves the imbibition efficiency (Wang et al., 2020). Following this, the imbibition efficiency significantly improves under the influence of enhanced capillary force and compaction. Taking S3 as an example, the imbibition curve rises slowly after 550 min of imbibition, while it basically ends after 4000 min of imbibition under 20 °C and 0.1 MPa, which indicates that the pressure affects the end time of imbibition. Increasing the imbibition pressure has a positive effect on improving the core imbibition recovery.

It can be seen that under the condition of constant control pressure, increasing the imbibition temperature obviously improves the imbibition recovery. In addition, when the temperature is controlled and the environmental pressure is increased, the oil recovery also increases. Therefore, increasing the temperature and pressure can promote oil recovery.

Fig. 10 compares the imbibition recovery of samples under different temperature and pressure conditions. The curves of the two samples under 60 °C and 4 MPa are above the curves of the samples at room temperature and pressure. The imbibition recovery rate of the sample under 60 °C and 4 MPa is higher than that of the sample under 20 °C and 4 MPa. The

Table 6. Classification of pore areas based on T_2 spectral values (Jiang et al., 2018).

Relaxation time (ms)	Pore diameter (nm)	Pore area
0.1~100	1~1000	Nano pore
≥ 100	≥ 1000	Microporous/Mesoporous

**Fig. 10.** Comparison of the influence of temperature and pressure of some cores on the permeability recovery.

imbibition recovery rate under 60 °C and 4 MPa increases obviously and reaches more than 10%.

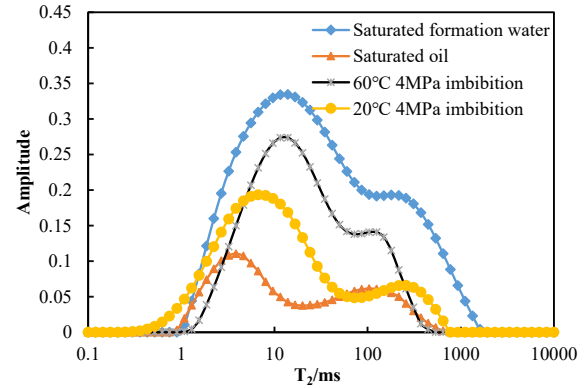
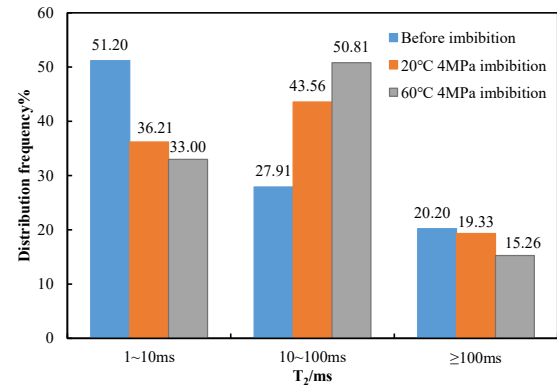
4.3 Fluid distribution under different temperatures and pressures

The pore size classification method proposed by Loucks et al. (2012) categorizes pore areas into nanopores (less than 1.0 μm), micropores (1.0~62.5 μm), and mesopores (62.5 μm ~4.0 mm). Based on the size of the T_2 spectrum, the aperture is mainly distributed in the following three intervals: 0.1~100 ms, 100~1000 ms, and ≥ 1000 ms. Based on the average value method, the conversion coefficient between the T_2 value and the pore diameter is calculated. Combined with the pore size classification method proposed by Loucks et al. (2012), pores can be classified directly according to the T_2 value, and the specific areas are listed in Table 6. For convenience, 0.1~1 ms is classified as nanomicro-pore, 1~10 ms is classified as nanomeso-pore, and 10~100 ms is classified as nano macro-pore (Jiang et al., 2018).

4.3.1 Effects of temperature

The influence of temperature on the fluid distribution in pores was obtained by observing the changes of T_2 spectra of cores before and after the imbibition experiments at 20 °C 4 MPa and 60 °C 4 MPa. Fig. 11 shows the T_2 spectrum of the S2 after the temperature change.

The amount of fluid in the nanomeso-pores is the largest, that is, the number of nanomeso-pores is the largest, followed by nano macro pores, micropores, mesopores, and finally, nanomicro-pores. In Fig. 11, the sample has good connectivity and is prone to imbibition. Most of the fluids are distributed in the nano pores (mainly in the nanomeso-pores and nano macro pores), with lesser amounts of imbibition fluids in the

**Fig. 11.** T_2 spectrum comparison of S2 after imbibition under different temperatures.**Fig. 12.** Distribution ratio of fluid in pores of S2 core before and after imbibition at different temperatures.

nanomicro-pores (less than 5% of the total). The rest of the fluids are distributed in the micropores and mesopores.

Fig. 12 shows the distribution frequency of fluids before and after imbibition under different conditions. It can be seen that the proportion of the nano macro-porous fluid increases significantly after imbibition, to about 50%, which indicates that the imbibition mainly occurs in the nanomacro-pores. With the increase in the temperature, the proportion of fluid in the nanomacro-pores increases from 43.56% to 50.81%, and the distribution frequency of fluids in other pores decreases to varying degrees, indicating that nanomacro-pores are more conducive to oil-water exchange with an increase in the temperature.

After imbibition under 20 °C and 4 MPa, the saturated oil is more stable than that before imbibition. The amount of fluid in the nanopores increases, but only by a small amount. The fluid is mainly distributed in the nanomeso-pores and

nano pores, accounting for 80% of the total. The pore size of the nano pore is the smallest and the capillary force is the strongest. Therefore, a small amount of formation water enters and displaces the crude oil in the pore. Because of the small pore size, strong capillary force, and the large number of nano macro pores, they contribute the most to the imbibition. The amount of nano mesoporous is the second highest, its capillary force is strong, which is also the main driver of the imbibition.

After increasing the temperature to 60 °C, the T_2 spectrum curve shifts to the right, and the fluid concentrates mainly in the nano macro pores and then in the nanomeso-pores. Compared with the T_2 value of the sample at 4 MPa at 20 °C, the fluid in the nanomeso-pore and nano macropore increases significantly. The reason for this is that with the increase in the temperature, the viscosity of the crude oil in the formation decreases, the fluidity of the crude oil increases, the connectivity improves, and the nano pore capillary force becomes stronger. Therefore, the amount of the nano pore fluid increases significantly, that is, the oil-water replacement in the formation mainly occurs here.

4.3.2 Effects of pressure

The T_2 spectrum of the samples after subjecting them to conditions of 20 °C at 0.1 MPa and 20 °C at 4 MPa show the characteristics of the fluid distribution in pores before and after imbibition under different pressures. The T_2 spectrum of the cores is also used to analyze the influence of pressure on fluid distribution in the pores. Fig. 13 shows the T_2 of the S2 core after imbibition under different pressures. The T_2 spectrum value of the saturated formation water reflects the pore distribution in the core. Because only the distribution of the H^+ ion is detected by NMR, the movable water distribution can reflect the general pore distribution.

The core is mainly composed of nanopores and micropores. The bimodal structure shows that the pores of different sizes have good connectivity, and that the nanopores are the main type of pore. Fig. 13 shows that after imbibition, the fluid in the pores is mainly distributed in the nanopores and micropores, accounting for about 80%. The reason for this is that the imbibition is mainly affected by the capillary force. The pore size of nano pores is small and the capillary force is strong. The number of nano pores is large, and the imbibition effect is obvious. The fluid distribution in different pore sizes is plotted in Fig. 14 to show the fluid changes more intuitively in different pore sizes.

The fluid content in the nanomeso-pores is the highest before imbibition, reaching 51.20%. It indicates that in the process of displacement, the formation water in the pores is displaced from the macro pores to the nano pores under the effect of the external displacement pressure. Therefore, the amount of the formation water in the nano pores is the largest. Under different pressures, the same core shows different imbibition characteristics. Compared with the imbibition under 0.1 MPa, the ratio of fluid in the nano pore is increased. The fluid content in all pores also increases because the increase in pressure has a positive effect on the recovery. The reason for highest amount of fluid in the nano-macropore can be explained by the higher pressure which favors more formation

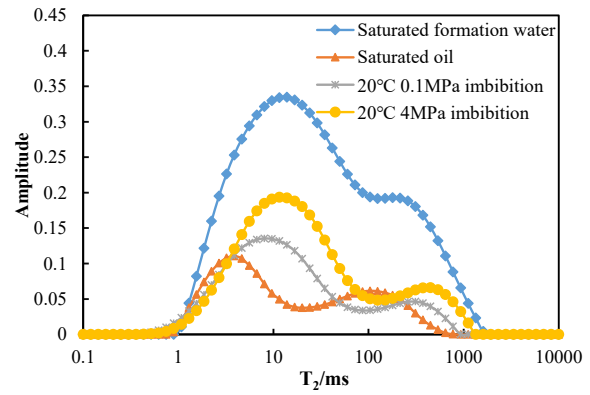


Fig. 13. T_2 spectrum comparison of S2 after imbibition under different pressures.

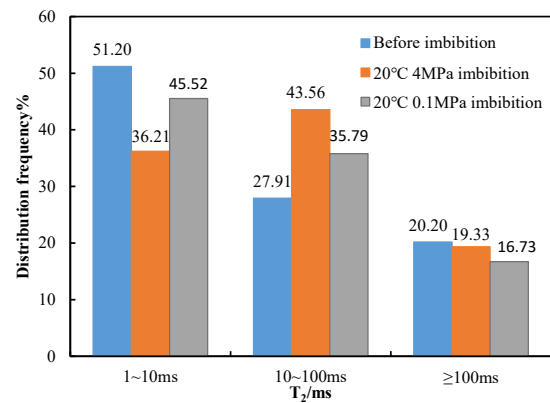


Fig. 14. Distribution ratio of fluid in pores before and after imbibition under different pressure conditions.

water to enter the pores due to the increase in external pressure. Meanwhile, a higher pressure causes deformation in pores, squeezing out the crude oil in the pores which provides more space for water to enter the oil-bearing pores. The reason for the small increase in mesoporous fluid can be explained by the compaction effects which discharge the crude oil in the pores, whereas formation water can not completely enter.

One conclusion can be obtained is that the largest amount of fluid infiltrates the nano pores, which dominates the imbibition at an elevated pressure. The amount of fluid in each type of pore in the core increases with increasing pressure. The amount of fluid in the nano macropore increases by about 10% for samples under 4 MPa compared with that under 0.1 MPa. Increasing pressure reduces the sizes of nano-pores due to the compaction effects, which explains the residual water volume in nanomacro-pores increasing from 36.79% to 43.56%. The significant increment in the portion of residual water in nanomacro-pores further leads to the decrease in the portion of residual water in nanomeso-pores.

5. Conclusions

- 1) The imbibition experiments on rock samples at 20 °C and 60 °C under 4 MPa pressure shows that the imbibition recovery increases by 10-15% with an increase in the

temperature.

- 2) The oil recovery increases by 3-5% with an increase in the pressure.
- 3) The imbibed water is mainly distributed in the nano-pores after the imbibition process. The nanomacro-pores play a dominate role in the imbibition of tight samples.
- 4) Increasing pressure increases the amount of irreducible water in the nano pores, with the relatively more significant increase in the amount of irreducible water in the nanomacro-pores compared with other types of pores.

Acknowledgments

We sincerely appreciate financial support from the National Natural Science Foundation of China (No. 51774255), the National Major Science and Technology Projects of China (No. 2017ZX05009-005), and the Fundamental Research Funds for the Central Universities (2-9-2018-210).

Conflict of interest

The authors declare no competing interest.

Open Access This article is distributed under the terms and conditions of the Creative Commons Attribution (CC BY-NC-ND) license, which permits unrestricted use, distribution, and reproduction in any medium, provided the original work is properly cited.

References

- Adibhatla, B., Mohanty, K. K. Parametric analysis of surfactant-aided imbibition in fractured carbonates. *Journal of Colloid and Interface Science*, 2008, 317(2): 513-522.
- Akbarabadi, M., Piri, M. Nanotomography of the spontaneous imbibition in shale. Paper URTEC 1922555 Presented at SPE/AAPG/SEG Unconventional Resources Technology Conference in Denver, Colorado, USA, 25-27 August, 2014.
- Aronofsky, J. S., Jenkins, R. A. Simplified analysis of unsteady radial gas flow. *Journal of Petroleum Technology*, 1954, 6(7): 23-28.
- Babadagli, T. Dynamics of capillary imbibition when surfactant, polymer, and hot water are used as aqueous phase for oil recovery. *Journal of Colloid and Interface Science*, 2002, 246(1): 203-213.
- Cai, J., Li, C., Song K., et al. The influence of salinity and mineral components on spontaneous imbibition in tight sandstone. *Fuel*, 2020, 269: 117087.
- Cai, J., Perfect, E., Cheng, C. L., et al. Generalized modeling of spontaneous imbibition based on Hagen–Poiseuille flow in tortuous capillaries with variably shaped apertures. *Langmuir*, 2014, 30(18): 5142-5151.
- Dou, L., Xiao, Y., Gao, H., et al. The study of enhanced displacement efficiency in tight sandstone from the combination of spontaneous and dynamic imbibition. *Journal of Petroleum Science and Engineering*, 2021, 199: 108327.
- Dou, L., Yang, M., Gao, H., et al. Characterization of the dynamic imbibition displacement mechanism in tight sandstone reservoirs using the NMR technique. *Geofluids*, 2020, 2020: 8880545.
- Fini, M. F., Riahi, S., Bahramian, A. Experimental and QSPR studies on the effect of ionic surfactants on n-decane-water interfacial tension. *Journal of Surfactants and Detergents*, 2012, 15(4): 477-484.
- Gao, Z. Y., Hu, Q. H. Investigating the effect of median pore-throat diameter on spontaneous imbibition. *Journal of Porous Media*, 2015, 18(12): 1231-1238.
- Ghasemi, F., Ghaedi, M., Escrochi, M. A new scaling equation for imbibition process in naturally fractured gas reservoirs. *Advances in Geo-Energy Research*, 2020, 4(1): 99-106.
- Gong, Y. B., Sedghi, M., Piri, M. Dynamic pore-scale modeling of residual trapping following imbibition in a rough-walled fracture. *Transport in Porous Media*, 2021, doi: <https://doi.org/10.1007/s11242-021-01606-1>. (in press)
- Hendraningrat, L., Torsater, O. Effects of the initial rock wettability on silica-based nanofluid-enhanced oil recovery processes at reservoir temperatures. *Energy & Fuels*, 2014, 28(10): 6228-6241.
- Hu, Y. F., Ren, F., Li, J., et al. Effect of dynamic imbibition on the development of ultralow permeability reservoir. *Geofluids*, 2021, 2021: 5544484.
- Jiang, Y., Shi, Y., Xu, G., et al. Experimental study on spontaneous imbibition under confining pressure in tight sandstone cores based on low-field nuclear magnetic resonance measurements. *Energy & Fuels*, 2018, 32(3): 3152-3162.
- Lai, F. P., Li, Z. P., Dong, H. K., et al. Micropore structure characteristics and water distribution in a coalbed methane reservoir. *Australian Journal of Earth Sciences*, 2019, 66(5): 741-750.
- Lai, F. P., Li, Z. P., Wei, Q., et al. Experimental investigation of spontaneous imbibition in a tight reservoir with nuclear magnetic resonance testing. *Energy & Fuels*, 2016, 30(11): 8932-8940.
- Li, K., Chow, K., Horne, R. N. Effect of initial water saturation on spontaneous water imbibition. Paper SPE 76727 Presented at SPE Western Regional/AAPG Pacific Section Joint Meeting in Anchorage, 20–22 May, 2002.
- Loucks, R. G., Reed, R. M., Ruppel, S. C., et al. Spectrum of pore types and networks in mudrocks and a descriptive classification for matrix-related mudrock pores. *AAPG Bulletin*, 2012, 96(6): 1071-1098.
- Ma, S., Morrow, N. R., Zhang, X. Generalized scaling of spontaneous imbibition data for strongly water-wet systems. *Journal of Petroleum Science and Engineering*, 1997, 18(3-4): 165-178.
- Mason, G., Fischer, H., Morrow, N. R., et al. Correlation for the effect of fluid viscosities on counter-current spontaneous imbibition. *Journal of Petroleum Science and Engineering*, 2010, 72(1-2): 195-205.
- McWhorter, D. B., Sunada, D. K. Exact integral solutions for two-phase flow. *Water Resources Research*, 1990, 26(3): 399-413.
- Meng, Q., Cai, J. Recent advances in spontaneous imbibition with different boundary conditions. *Capillarity*, 2018, 1(3): 19-26.

- Mohammadi, S., Kord, S., Moghadasi, J. An experimental investigation into the spontaneous imbibition of surfactant assisted low salinity water in carbonate rocks. *Fuel*, 2019, 243: 142-154.
- Nasralla, R. A., Bataweel, M. A., Nasr-El-Din, H. A. Investigation of wettability alteration and oil-recovery improvement by low-salinity water in sandstone rock. *Journal of Canadian Petroleum Technology*, 2013, 52(2): 144-154.
- Schechter, D. S., Zhou, D., Orrjr, F. M. Low IFT drainage and imbibition. *Journal of Petroleum Science and Engineering*, 1994, 11(4): 283-300.
- Schmid, K. S., Geiger, S. Universal scaling of spontaneous imbibition for arbitrary petrophysical properties: Water-wet and mixed-wet states and Handy's conjecture. *Journal of Petroleum Science and Engineering*, 2013, 101: 44-61.
- Schmid, K. S., Geiger, S., Sorbie, K. S. Semianalytical solutions for cocurrent and countercurrent imbibition and dispersion of solutes in immiscible two-phase flow. *Water Resources Research*, 2011, 47(2): 2144-2150.
- Shen, A., Liu, Y., FarouqAli, S. M. A model of spontaneous flow driven by capillary pressure in nanoporous media. *Capillarity*, 2020, 3(1): 1-7.
- Sohi, M. L., Sola, B. S., Rashidi, F. Experimental investigation of effective parameters on efficiency of capillary imbibition in naturally fractured reservoirs. *Journal of the Japan Petroleum Institute*, 2009, 52(2): 36-41.
- Tinni, A., Odusina, E., Sulucarnain, I., et al. Nuclear-magnetic-resonance response of brine, oil, and methane in organic-rich shales. *SPE Reservoir Evaluation & Engineering*, 2015, 18(3): 400-406.
- Wang, C., Gao, H., Gao, Y., et al. Influence of pressure on spontaneous imbibition in tight sandstone reservoirs. *Energy & Fuels*, 2020, 34(8): 9275-9282.
- Wang, X. K., Sheng, J. J. Dynamic pore-scale network modeling of spontaneous water imbibition in shale and tight reservoirs. *Energies*, 2020, 13(18): 4709.
- Washburn, E. W. The dynamics of capillary flow. *Physical Review*, 1921, 17(3): 273-283.
- Xu, X., Wan, Y. J., Li, X., et al. Microscopic imbibition characterization of sandstone reservoirs and theoretical model optimization. *Scientific Reports*, 2021, 11(1): 8509.
- Yang, L., Ge, H., Shen, Y., et al. Experimental research on the shale imbibition characteristics and its relationship with microstructure and rock mineralogy. Paper SPE 176882 Presented at SPE Asia Pacific Unconventional Resources Conference and Exhibition in Brisbane, Brisbane, Australia, 9-11 November, 2015.
- Yildiz, H. O., Gokmen, M., Cesur, Y. Effect of shape factor, characteristic length, and boundary conditions on spontaneous imbibition. *Journal of Petroleum Science and Engineering*, 2006, 53(3-4): 158-170.
- Zhang, X., Morrow, N. R., Ma, S. X. Experimental verification of a modified scaling group for spontaneous imbibition. *SPE Reservoir Engineering*, 1996, 11(4): 280-285.
- Zou, C. N., Yang, Z., He, D. B., et al. Theory, technology and prospects of conventional and unconventional natural gas. *Petroleum Exploration and Development*, 2018, 45(4): 604-618.